Journal of Biomechanics 43 (2010) 2149–2158

Contents lists available at ScienceDirect

Journal of Biomechanics

journal homepage: www.elsevier.com/locate/jbiomech
www.JBiomech.com

Automatic segmentation of surface EMG images: Improving the estimation of neuromuscular activity

Taian M.M. Vieira [a,b,*], Roberto Merletti [a], Luca Mesin [a]

[a] Laboratory for Engineering of the Neuromuscular System, Politecnico di Torino, Torino, Italy
[b] School of Physical Education and Sports, Federal University of Rio de Janeiro, Rio de Janeiro, Brazil

ARTICLE INFO

Article history:
Accepted 29 March 2010

Keywords:
Electromyography
Image segmentation
Gastrocnemius
Neuromuscular compartments

ABSTRACT

Surface electromyograms (EMGs) recorded with a couple of electrodes are meant to comprise representative information of the whole muscle activation. Nonetheless, regional variations in neuromuscular activity seem to occur in numerous conditions, from standing to passive muscle stretching. In this study, we show how local activation of skeletal muscles can be automatically tracked from EMGs acquired with a bi-dimensional grid of surface electrodes (a grid of 8 rows and 15 columns was used). Grayscale images were created from simulated and experimental EMGs, filtered and segmented into clusters of activity with the watershed algorithm. The number of electrodes on each cluster and the mean level of neuromuscular activity were used to assess the accuracy of the segmentation of simulated signals. Regardless of the noise level, thickness of fat tissue and acquisition configuration (monopolar or single differential), the segmentation accuracy was above 60%. Accuracy values peaked close to 95% when pixels with intensity below ~70% of maximal EMG amplitude in each segmented cluster were excluded. When simulating opposite variations in the activity of two adjacent muscles, watershed segmentation produced clusters of activity consistently centered on each simulated portion of active muscle and with mean amplitude close to the simulated value. Finally, the segmentation algorithm was used to track spatial variations in the activity, within and between medial and lateral gastrocnemius muscles, during isometric plantar flexion contraction and in quiet standing position. In both cases, the regionalization of neuromuscular activity occurred and was consistently identified with the segmentation method.

1. Introduction

Surface electromyography advanced rapidly in the last decade, in particular regarding the development of sophisticated detection systems, which currently comprise grids with hundreds of electrodes (Merletti et al., 2009).

The conventional bipolar configuration may suffice for identifying gross activation of skeletal muscles in specific motor tasks (Danion et al., 2002; McLean and Goudy, 2004), or in response to stretching stimuli (Schieppati et al., 2001). Conversely, this configuration provides unrepresentative electromyograms (EMGs) if the location of surface electrodes is not chosen properly. Indeed, variations in amplitude and spectral features of surface EMGs, with respect to the position of electrodes, have been extensively studied using arrays of electrodes (Farina et al., 2002; Mesin et al., 2009; Merletti et al., 2003; Zwarts and Stegeman, 2003). Spurious changes in EMG traces hinder the observation of neuromuscular activity when surface electrodes are placed close to the innervation zone or the tendon locations (Mesin et al., 2009).

Quantifying muscle activity with a linear array or pairs of electrodes presumes that the whole muscle is activated homogeneously. Such an assumption is particularly relevant when estimating muscle forces with analytical models (Lloyd and Besier, 2003; Zajac, 1989). Nonetheless, compelling evidences indicate that skeletal muscles are functionally divided into compartments, activated selectively in voluntary contractions (Danion et al., 2002; McLean and Goudy, 2004), during the control of quiet standing posture (Vieira et al., 2010), and even in response to muscle stretching (Eng and Hoffer, 1997). Therefore, the assessment of neuromuscular activity in different motor tasks would benefit from the use of bi-dimensional arrays of electrodes, allowing for the identification of localized EMG activity within and between muscles.

In this study, we propose and validate a method for the automatic identification of local variations in surface EMG activity with a bi-dimensional array of electrodes. Initially, the generation of scaled images from the surface EMGs is outlined. Then, EMG

* Corresponding author at: Dipartimento di Elettronica, Politecnico di Torino, Corso Duca degli Abruzzi 24, Torino 10129, Italy. Tel.: 39 011 4330476; fax: 39 011 4330404.
E-mail address: taian.vieira@delen.polito.it (T.M. Vieira).

0021-9290/$ - see front matter © 2010 Elsevier Ltd. All rights reserved.
doi:10.1016/j.jbiomech.2010.03.049

images are segmented with the watershed algorithm (Vincent and Soile, 1991). The performance of our method is assessed using simulated EMGs. Finally, we applied the method to segment experimental signals recorded from the gastrocnemius muscles. We chose these muscles because of their high degree of compartmentalization (English et al., 1993) and our interest in understanding how such a partitioning might affect the control of human standing posture (Vieira et al., 2009, 2010). The segmentation method proposed here is expectedly useful to study localized muscle activity, the load sharing between synergists and to predict muscle force using EMG-driven models.

2. Methods

2.1. Generating images from surface EMG signals

When electromyograms are recorded with a bi-dimensional grid of electrodes, each electrode may be conceived as a pixel p with coordinates x and y given by the rows and columns in the grid. EMG activity is often represented with its average rectified value (ARV) or its root mean square (RMS). For EMG images generated with the ARV descriptor, pixels intensity is computed as

$$I_{emg}[x,y,\ i] = \frac{1}{N}\sum_{n\,=\,1+(i-1)N}^{iN} |EMG[x,y,n]| \tag{1}$$

where i and N stand for the epoch number and the number of samples in each epoch, respectively. In a grayscale EMG image, dark and light pixels indicate low and high EMG amplitudes, respectively (Fig. 1).

The cluster of pixels with high intensity in Fig. 1 means a group of electrodes detecting high EMG activity and likely reflects the spatial selectivity of muscle activation.

2.2. Segmenting EMG image with watersheds

The watershed technique segments grayscale images by considering pixels with high intensity as elevated surfaces and pixels with low intensity as catchment basins. Similarly, the intensity of pixels in EMG images can be represented as a topographical relief (Fig. 2). The algorithm identifies the location of ridges (watersheds) in the grayscale image and labels each catchment basin (group of pixels), surrounded by such ridges, with a different number (Vincent and Soile, 1991).

Since pixels with high ARV amplitude would be conceived as elevated surfaces, clusters of these pixels would be partitioned if the watershed algorithm was applied directly to EMG images (Fig. 2a). In this case, pixels with high gray intensity (i.e. high neuromuscular activity) would constitute the watershed line, which is not desired. Rather, watershed lines could be estimated by processing the gradient of I_{emg}. Assuming that pixels represent the spatial sampling of I_{emg}, the edges of subsets with low and high EMG activities are computed as the Euclidean norm of I_{emg} gradient (g_{emg}), which gives the rate of change in gray intensity (Fig. 2b)

$$\begin{aligned} g_x[m,\ n;\ i] &= F^{-1}\left[S^T \sum_{m\,=\,1}^{N_r}\sum_{n\,=\,1}^{N_c} I_{emg}[m,n;\ i] e^{-j2\pi\left(\frac{k_x m}{N_r}+\frac{k_y n}{N_c}\right)}\right] \\ g_y[m,n;i] &= F^{-1}\left[S \sum_{m\,=\,1}^{N_r}\sum_{n\,=\,1}^{N_c} I_{emg}[m,n;\ i] e^{-j2\pi\left(\frac{k_x m}{N_r}+\frac{k_y n}{N_c}\right)}\right] \\ g_{emg} &= \sqrt{g_x^2+g_y^2} \end{aligned} \tag{2}$$

where F^{-1} is the inverse of the Fourier transform operator, k_x and k_y indicate the spatial frequencies, N_r and N_c stand for the number of rows and columns of electrodes, T indicates the transpose operator, and S is the bi-dimensional Fourier transform of the zero-padded Sobel operator

$$s = \begin{vmatrix} +1 & +2 & +1 \\ 0 & 0 & 0 \\ -1 & -2 & -1 \end{vmatrix} \tag{3}$$

As the number of clusters produced by the watershed segmentation depends on the number of regional minima in the gradient, the problem of over-segmentation (Fig. 2b) can be minimized by flattening sharp transitions of gray intensity in g_{emg} with image opening followed by image closing operation (Heijmans, 1995). Opening and closing can be envisaged as the attenuation and intensification of pixels with intensity exceeding or not reaching some threshold, respectively. Opening and closing g_{emg} by the structuring element v are defined as (Heijmans, 1995)

$$g_{emg} \circ v = (g_{emg} \ominus v) \oplus v \tag{4}$$

$$g_{emg} \bullet v = (g_{emg} \oplus v) \ominus v \tag{5}$$

where $\circ$ and $\bullet$ indicate opening and closing, respectively. $\oplus$ and $\ominus$ are the Minkowski operators for addition and difference, defined as

$$(g_{emg} \oplus v)(p) = \max_{z\,\in\,D_v}\{g_{emg}(p+z)\} \tag{6}$$

$$(g_{emg} \ominus v)(p) = \min_{z\,\in\,D_v}\{g_{emg}(p+z)\} \tag{7}$$

where D_v is the domain of the structuring element v, which was chosen as a square grid (3×3) of zeros (which means that $z \in [-1,0,1]\times[-1,0,1]$).

The opened–closed gradient of I_{emg} provided a flattened surface for the segmentation. Clusters of EMG activity were then identified properly with the watershed algorithm (Fig. 2c).

Enhancing the contrast of EMG image with histogram equalization (Kim et al., 2001), before computing its gradient, emphasized groups of pixels with similar intensity and further improved the watershed segmentation (Fig. 2d).

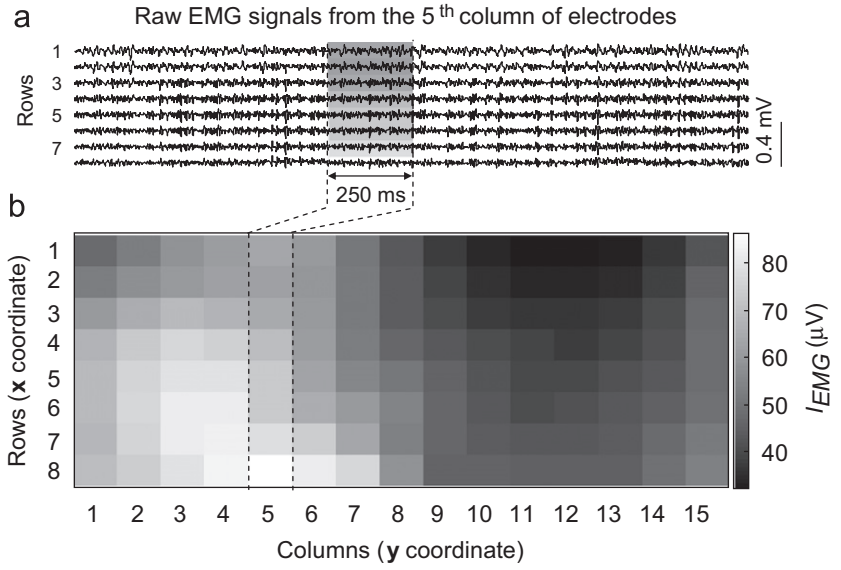

Fig. 1. Grayscale image (bottom panel) created with intensity values (I_{emg}) computed for experimental EMGs recorded from the gastrocnemius muscles during isometric plantar flexion (Section 2.3.2). A matrix of 120 electrodes, disposed into 8 rows and 15 columns, was used for the EMGs acquisition. Pixels intensity corresponds to ARV amplitudes computed for an epoch of 250 ms (dashed lines).

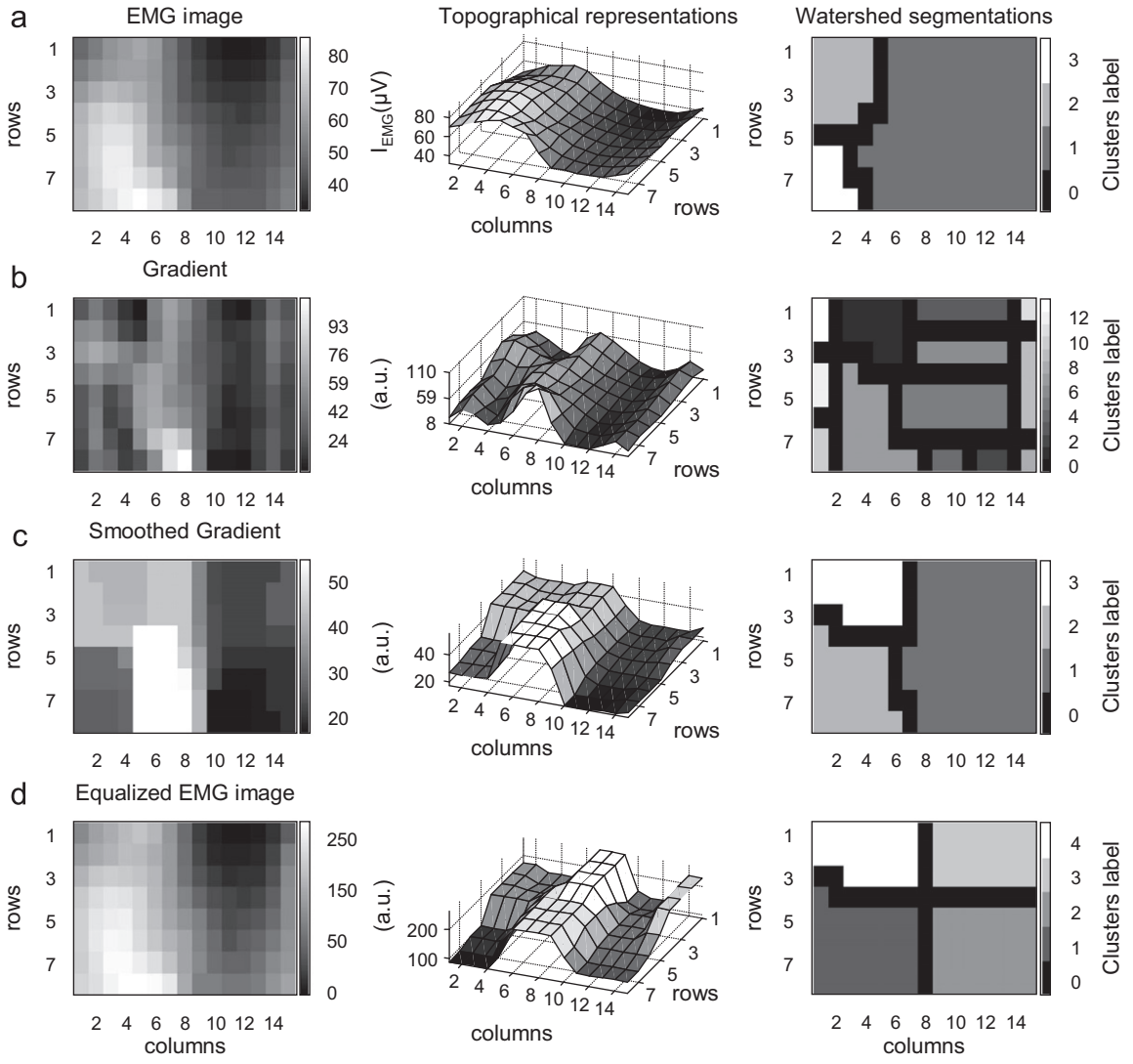

Fig. 2. Schematic of watershed segmentation (right panels) applied to: (a) the grayscale image created with ARV amplitude of experimental EMG signals, as shown in Fig. 1; (b) the gradient (Eq. (2)) of the image shown in (a); (c) the flattened gradient, obtained with image opening and image closing techniques (Eqs. (3) and (4)); (d) the flattened gradient estimated as in (c) but for the equalized EMG image. Surfaces shown in the middle panels comprise a topographical representation of EMG image and its gradients shown in the left panel, except in (d), where the topographical representation (middle panel) refers to the flattened gradient of the equalized EMG image (left panel).

This equalization technique stretches the intensity distribution across the range of values used to represent EMG amplitude as gray intensity (from 0 to 255), with dark and bright regions becoming even darker and brighter (left panel in Fig. 2a,d).

After partitioning EMG images into clusters of pixels with similar activity levels, the maximal ARV amplitude was calculated for each cluster. Electrodes corresponding to pixels with intensity below some threshold, from 0% to 90% of maximal ARV amplitude, were further excluded from each cluster.

2.3. Signals used for EMG segmentation testing and analysis

The proposed segmentation method was tested for simulated and experimental EMGs.

2.3.1. Simulated signals

Monopolar surface EMGs were simulated by positioning muscle fibers inside a rectangular cross-section area of 100 mm × 15 mm (Fig. 3a). The parameters in Table 1 were used to generate interference EMGs (Fig. 3b). EMG images were created and then segmented with the proposed algorithm (Fig. 3c,d).

The segmentation algorithm was tested for two simulation sets, each with 30 different populations of motor units.

First set: one muscle 60 mm large was simulated active at 60% of maximal voluntary contraction (MVC) and with fat thickness varying between 2 and 6 mm.

Second set: two adjacent muscles with identical dimensions (50 mm large) were simulated active. The force level varied from 10% to 90% MVC for the first muscle and from 90% to 10% MVC for the second muscle, giving an average force level of 50% MVC. The contiguous location of both muscles was simulated to reproduce the two gastrocnemius muscles.

2.3.2. Experimental signals

Experimental EMGs were used to investigate the feasibility of the proposed algorithm in identifying clusters of activity within and between medial (MG) and lateral (LG) gastrocnemius. Monopolar signals were detected from eight healthy subjects (18–36 years) with a matrix of 8 × 15 electrodes. After cleansing and wetting the skin with alcohol and water, the electrodes were placed exclusively above the gastrocnemius muscles, as confirmed by ultrasound imaging (Vieira et al., 2010; see supplemental material). Basically, the junction between both muscles and their contours were scanned by sliding the ultrasound probe on the leg and marked on the skin. Each half of the matrix was then positioned on each gastrocnemius muscle (Fig. 6a). Ultrasound imaging was also used to estimate the fat thickness, which ranged from 3.4 to 5.6 mm. These values were within the simulated range of fat thickness, from 2 to 6 mm.

ARV maps were created for EMGs recorded synchronously with: (1) ankle torque during 10 s of isometric plantar flexion at 60% MVC, once with knee extended and once with knee flexed (Vieira et al., 2008); (2) centre of pressure during 40 s of quiet standing (Vieira et al., 2010). EMGs were amplified by

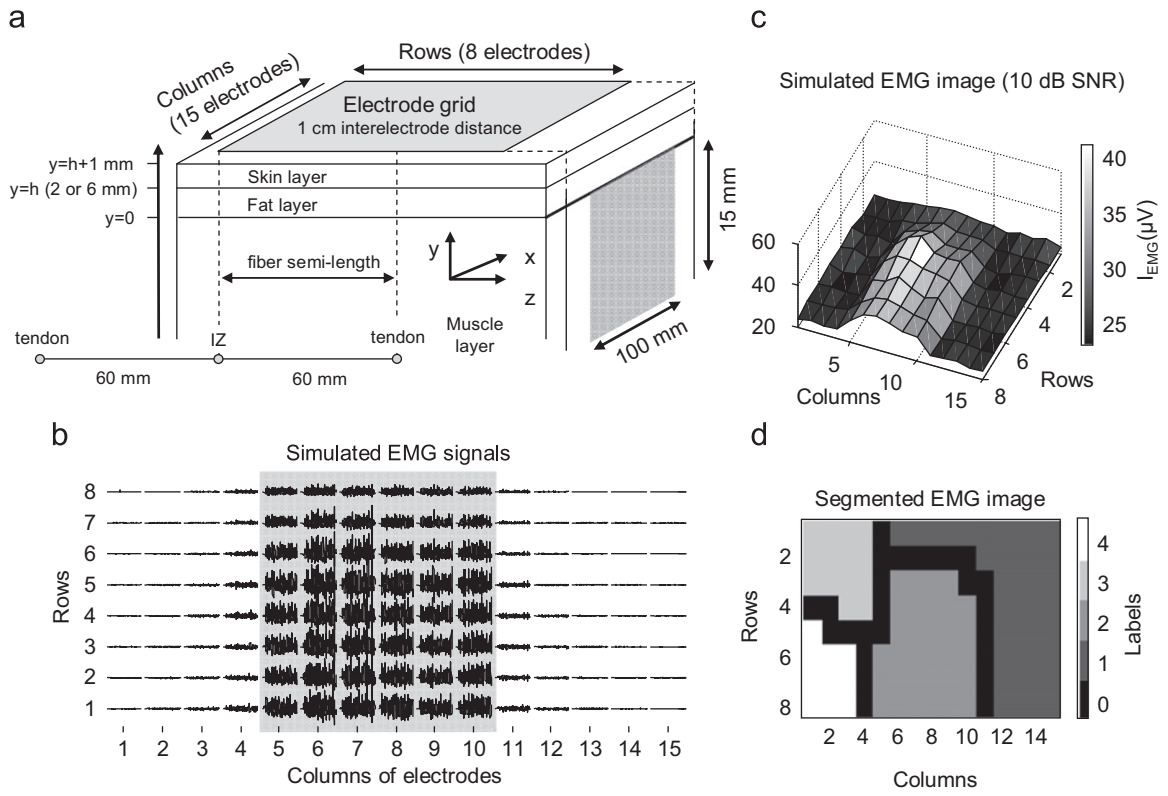

Fig. 3. (a) Schematic and specifications of the simulated muscle portion and of the grid of electrodes. The shaded area corresponds to the portion of muscle for which fiber potentials were simulated. (b) Example of raw monopolar EMGs simulated for the muscle configuration shown in (a). (c) Topographical representation of EMGs shown in (b), after adding 10 dB SNR of Gaussian noise. (d) Watershed segmentation (as described in Section 2.2) of the topographical image shown in (c).

Table 1
Description of the parameters used to simulate interference EMGs (SD means standard deviation; Fuglevand et al., 1993). EMGs were simulated using the planar model proposed in Farina and Merletti (2001).

Parameter	Value
Skin conductivity	4.3×10^{-4} S/m
Fat conductivity	4.0×10^{-2} S/m
Muscle longitudinal conductivity	40×10^{-2} S/m
Muscle axial conductivity	9.0×10^{-2} S/m
Fiber mean length	120 mm
Spread of innervation zone	1 mm SD of Gaussian distribution
Spread of tendon endings	2 mm SD of Gaussian distribution
Fiber density	20 fibers per mm^2
Fiber depth	From 0.15 to 15 mm
Motor unit (MU) dimension	Exponential distribution of number of fibers per MU, with ten-fold variation between smallest and largest MUs
Conduction velocity (CV)	Gaussian distribution with 4 m/s mean and 0.3 m/s SD
Recruitment order	From low to high CV
Force level where recruitment stops	60% of maximal voluntary contraction (MVC)
Range of discharge rate	8–30 pulses per second (pps)
Variation in discharge rate with force	0.5 pps/%MVC
Inter-pulse interval variability	Gaussian distribution with coefficient of variation 0.2

5 k (10–500 Hz EMG-USB amplifier, LISiN and OTBioelettronica, Turin) and sampled at 2048 Hz with a 12 bit A/D converter (± 2.5 V dynamic range).

2.4. Segmentation performance and statistical analysis

The accuracy of segmentation of simulated EMG images was evaluated as the ratio between the sum of true positive and true negative electrodes and the total number of electrodes in the grid (120 for monopolar and 105 for differential configuration). This definition accounts for the two main classification errors. For example, if the watershed lines confine a large cluster, including electrodes above muscle portions not activated, the accuracy will not be high because of pixels falsely classified as positive. Similarly, if the cluster resulting from the segmentation does not comprise all electrodes above the active muscle portion, the accuracy will be low because of false negative pixels.

Three different methods were considered for the segmentation of EMG images: watershed without equalization, watershed with equalization and the segmentation without watershed. In the later case, clusters of EMG activity were formed by selecting pixels with amplitude higher than a threshold (Threshold method). The segmentation accuracy of simulated EMG images was evaluated by considering five SNR values (0, 5, 10, 15 and 20 dB), the three segmentation methods, two detection systems (monopolar and differential), and two thicknesses of the fat layer (2 and 6 mm). For each case, accuracy was computed for amplitude thresholds varying from 0% to 90% of maximal ARV, at steps of 5%. A multi-factorial

ANOVA was considered for such comparisons (first simulation set). For the second simulation set, the performance of watershed segmentation was evaluated by comparing simulated and estimated variations in activity for each of the two muscles.

3. Results

3.1. Simulation 1: single muscle

Clusters of EMG activity were identified more accurately with than without using the watershed algorithm (Fig. 4). However, regardless of the detection system simulated and independent of usage of the watershed algorithm, the accuracy of EMG image segmentation significantly depended on the noise level ($p=0.001$) and amplitude threshold, especially for low thresholds (Fig. 4).

The equalization of EMG images significantly improved the performance and robustness of watershed segmentation. Interestingly, for all conditions simulated, the accuracy peaked at the same amplitude threshold when segmenting equalized EMG images. Even when setting the amplitude threshold to 0%, watershed segmentation of equalized images was remarkably accurate (Fig. 4). By pooling the amplitude thresholds, watershed segmentation performed statistically better with than without image equalization. This improved performance was evident for low SNR, with the use of equalization leading to mean accuracy values higher than 80% for 0 dB SNR. Non-equalized images,

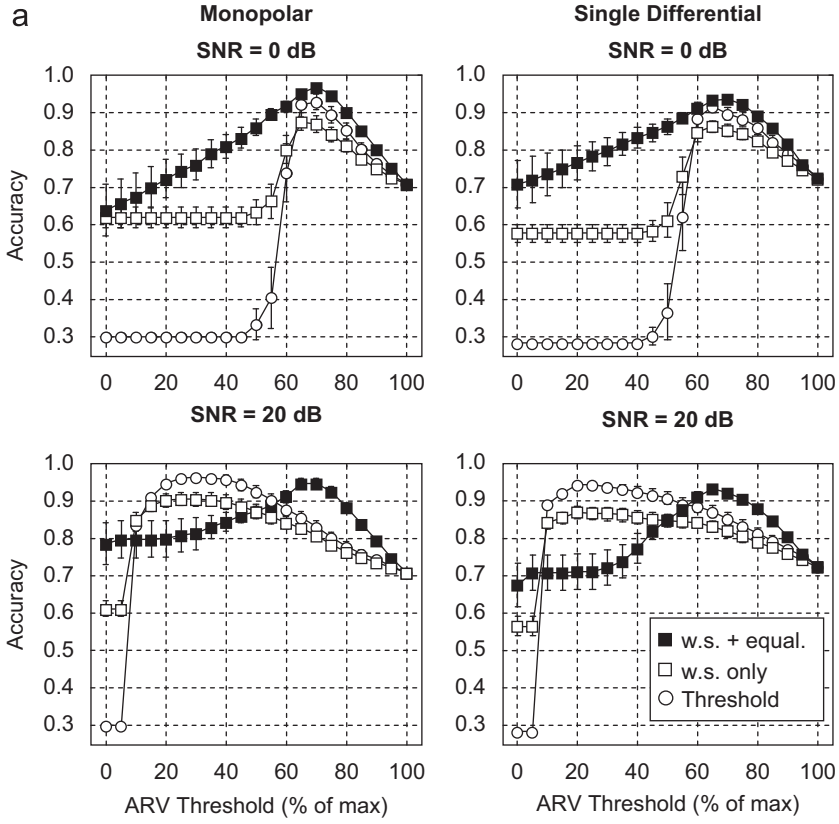

Fig. 4. First simulation set (Section 2.3.1). (a) The accuracy of classification of electrodes (mean values and confidence interval), covering (true positives) and not covering (true negative) the simulated portion of active muscle is shown for the segmentation of EMG images, as a function of the ARV threshold above which electrodes are considered. Thirty populations of motor units were simulated. Accuracy values are shown for the watershed segmentation with (■) and without (□) equalization, and without the use of watershed segmentation (○; threshold method). Accuracy values are reported for monopolar (left panels) and single differential (right panels) configurations and for SNR levels of 0 (upper panels) and 20 dB (bottom panels).

Table 2
Mean values (SD) of the accuracy (%) of EMG image segmentation when the watershed method was applied with (*eq*) and without (*non-eq*) histogram equalization. EMG images were created from simulated signals ($n=30$ sets of signals) with the fat thickness adjusted at 2 and 6 mm and with 0, 5, 10, 15, and 20 dB SNR.

	Monopolar				Single differential			
	Fat layer 2 mm		Fat layer 6 mm		Fat layer 2 mm		Fat layer 6 mm	
SNR	*eq*	*non-eq*	*eq*	*non-eq*	*eq*	*non-eq*	*eq*	*non-eq*
0	82 (13)*	70 (12)	83 (10)*	72 (13)	83 (10)*	68 (13)	83 (11)*	67 (15)
5	84 (11)*†	74 (12)†	86 (07)*	77 (13)	78 (14)*	76 (11)	80 (12)*	73 (14)
10	84 (10)*†	79 (11)†	88 (05)*	81 (12)	77 (14)†	77 (11)	82 (10)*	78 (12)
15	84 (10)*†	81 (10)†	88 (06)*	84 (11)	78 (13)†	80 (10)	82 (11)	82 (10)
20	85 (10)I	83 (09)†	89 (05)*	86 (10)	80 (12)	81 (08)	82 (10)	84 (09)

* $p<0.05$ between *eq* and *non eq* conditions
† $p<0.05$ between 2 and 6 mm fat thickness

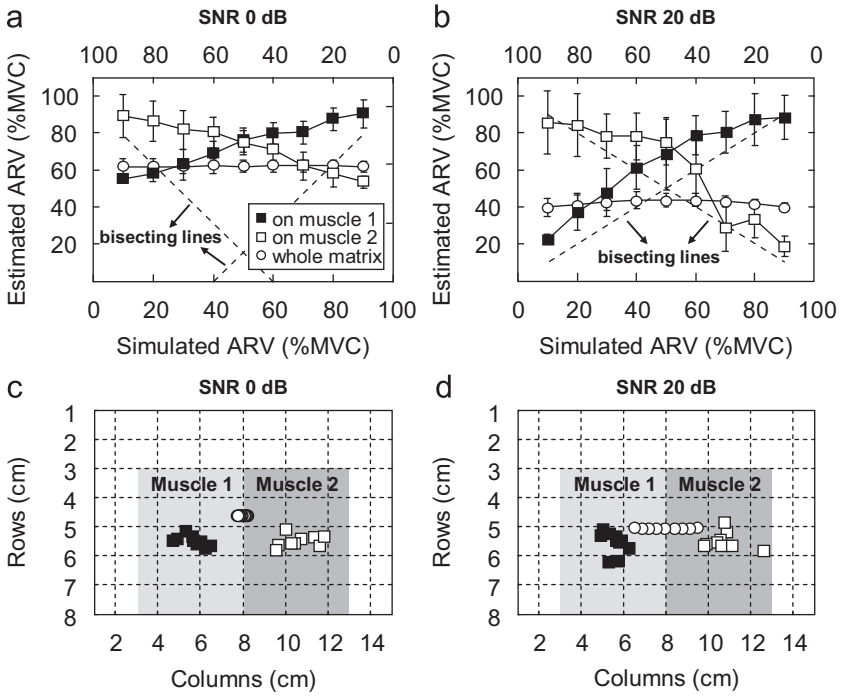

Fig. 5. Second simulation set (Section 2.3.1). Mean values and standard deviations (whiskers) of ARV amplitude (a and b; relative units, % of maximal ARV amplitude) and centroid coordinates (c and d), computed for the two clusters with highest activity (filled and unfilled squares). Such clusters were obtained using the watershed algorithm applied to the flattened gradient of equalized EMG images, with the amplitude threshold set at 70% of maximal ARV and for each epoch and for each set of simulated signals. Note that the position of the clusters is within the borders of the two simulated muscles (indicated with shaded areas for: muscle 1—left; muscle 2—right). Unfilled circles represent mean ARV values and centroid position estimated without segmentation of EMG image.

however, resulted in average accuracy lower than 75% for 0 and 5 dB SNR (Table 2). Similarly, segmentation of EMG images was slightly but significantly more accurate for thicker (84.3%) than thinner fat layer (81.5%; Table 2).

3.2. Simulation 2: two muscles

Variations in the level of activity of two closely spaced muscles were tracked appropriately with the watershed algorithm. When simulating simultaneous and opposite variations in activity of two adjacent muscles, the average EMG amplitude was almost constant (Fig. 5a,b). However, the watershed segmentation of equalized EMG images identified two clusters of activity. The average activity of each cluster approached the simulated effort level, although with overestimation for low SNR (Fig. 5a,b). The centroid of such clusters was located within the active muscle region. Conversely, the centroid of the whole EMG images shifted transversally as the activity of each muscle varied oppositely (Fig. 5c,d).

3.3. Experimental signals

The segmentation of experimental EMG images identified consistent and localized activity in each gastrocnemius muscle during isometric plantar flexion (Figs. 6,7). Considering one EMG frame, the watershed segmentation produced two large clusters of pixels. Pixels along the watershed line coincided with the location of the junction between both gastrocnemii, as confirmed with ultrasound imaging (Fig. 6a). After excluding pixels with intensity below 70% of maximal ARV, the clusters of electrodes were fairly localized over each muscle (Fig. 6b). Such localized activation of each gastrocnemius muscle was observed, consistently, when segmenting EMG frames throughout the 10 s of plantar flexion with knee extended and flexed (Fig. 7). Activation of both muscles was chiefly augmented in knee flexed condition, with the extent of activity in LG exceeding that in MG muscle.

Local variations in activity within the same gastrocnemius muscle were consistently identified when subjects stood at ease (Fig. 8). Segmentation of EMG images obtained during standing resulted into two clusters of activity, both centered mostly on MG muscle, proximally and distally (Fig. 8a). Fluctuations in ARV amplitude were remarkably similar to changes in CoP position, with distal and proximal clusters exhibiting more tonic and phasic activities, respectively (Fig. 8b).

4. Discussion and conclusions

In this study, we propose a method for the automatic segmentation of surface EMG images. Regardless of the activation level, active portions of simulated muscle were accurately identified with the segmentation method. Furthermore, segmentation of experimental EMG images revealed localized activity within and between gastrocnemius muscles.

4.1. Technical issues

Segmentation accuracy depends on the occurrence of false positive and false negative pixels. False positives correspond to electrodes positioned above inactive muscle portion and included in the cluster after segmentation. Electrodes over active muscle portion and not included in the cluster are false negatives. Once the watershed segmentation identifies cluster of EMG activity, the occurrence of false negative pixels cannot be corrected by raising the amplitude threshold. Conversely, false positive pixels might be excluded from the cluster if the amplitude threshold is raised progressively. This explains the increase in accuracy values for the segmentation of simulated EMG images when the amplitude

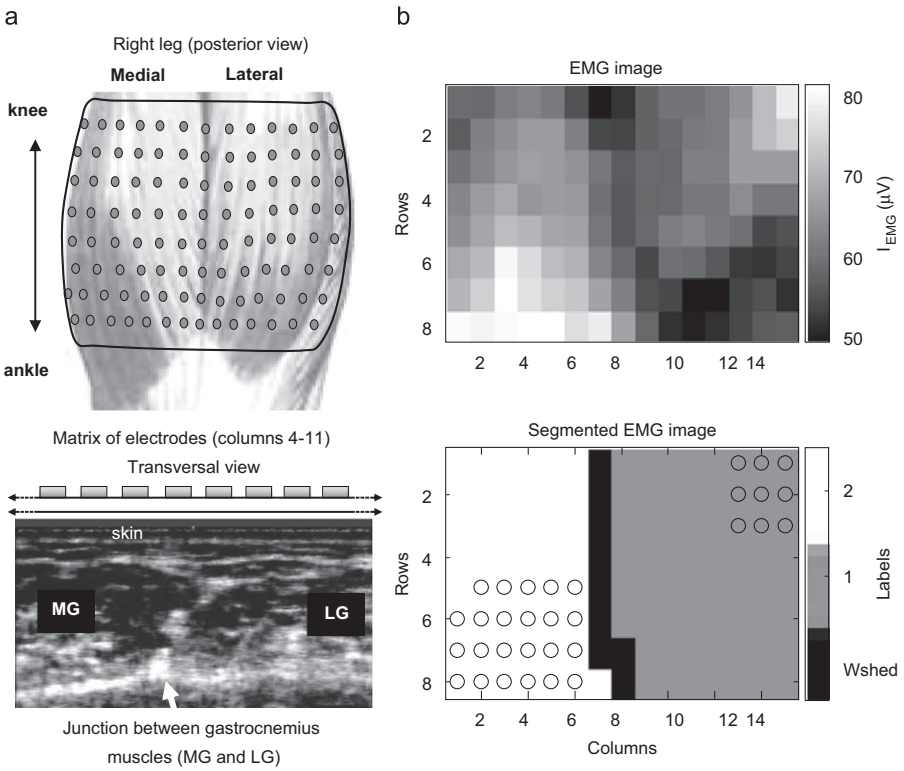

Fig. 6. (a) Positioning of the grid of 120 eyelet electrodes on the gastrocnemius muscles of the right calf. The ninth column of the grid was aligned with respect to the junction between the two muscles, identified with ultrasound imaging. (b) EMG image and segmentation of EMG equalized image with the watershed segmentation described in Section 2.2. By flattening the segmented image with image opening and closing and excluding pixels with intensity below 70% of maximal ARV amplitude, two clusters of high EMG activity are identified for each gastrocnemius muscle. Circles in the segmented image mark the final result of the segmentation procedure and thus define the regions of activity.

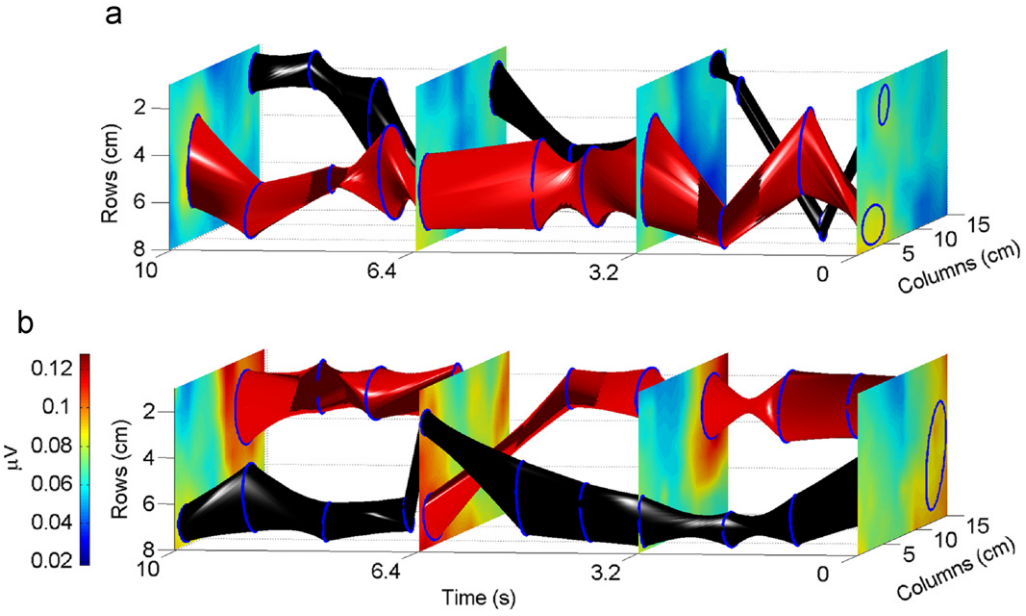

Fig. 7. Four EMG frames are shown for 10 s of isometric plantar flexion with knee extended (a) and knee flexed (b). Each frame was created with the ARV amplitude computed for 0.25 s epochs and for 120 monopolar signals recorded from the gastrocnemius muscles. The ninth column marks the junction between MG and LG muscles, as in Fig. 6. Blue ellipses were adjusted to the cluster of electrodes to produce a smooth visualization of localized activity with time. The direction of the major and minor axes of each ellipse was estimated with the two eigenvectors of the covariance matrix calculated for the electrode coordinates in each cluster. The length of each axis was then scaled with the corresponding eigenvalues. These ellipses were interpolated with elliptic cylinders to illustrate the time course of spatial variations in neuromuscular activity. Red and black cylinders denote the first and the second cluster with highest EMG activity, respectively. Note that the mean position of the cluster with highest activity changes from MG to LG muscle when comparing knee extended with knee flexed conditions.

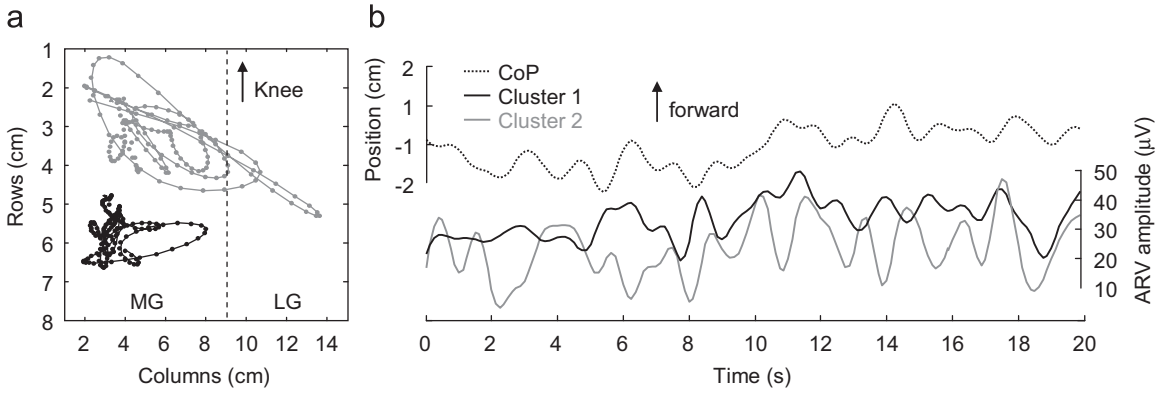

Fig. 8. (a) Coordinates of the centroid of the two clusters with highest activity, depicted for 20 s of quiet standing test. Dashed line shows the junction between MG and LG muscles. Note two distinct locations of activity, mostly on MG muscle. (b) Centre of pressure position in the sagittal plane and mean ARV amplitude, computed for the clusters whose centroid positions are shown in (a). Black and gray ARV traces correspond to the most distal and proximal clusters, respectively. Note that EMG activity in proximal portions fluctuates more than in the distal portion and with different timings.

threshold increased (Fig. 4). After all false positives are excluded from the cluster, any further increase in amplitude threshold excludes true positive pixels and thus decrease accuracy (Fig. 4). Therefore, the maximal accuracy relates inversely to the number of false negative pixels and matches the optimal amplitude threshold. Even without setting amplitude thresholds, the accuracy of watershed segmentation applied after equalization was fairly good (Fig. 4). Considering that accuracy peaked close to 0.95, consistently at ~70% amplitude threshold, the equalization led to robust and accurate identification of localized EMG activity (Fig. 4).

The preceding argument likely explains the higher accuracy obtained for thicker fat layers (Table 2). As increase in fat thickness leads to larger spread of action potentials on the skin (Farina et al., 2002, 2004), the segmentation of simulated EMG images resulted in clusters with less false negatives for thicker fat layer.

4.2. Interpreting the accuracy of simulated EMG segmentation

How much the accuracy of watershed segmentation of simulated signals translates into physiological values is predictable. The spatial spread of surface EMGs recorded from pinnated muscles is proportional to the number of active motor units (Vieira et al., 2010), and the distance between muscle fibers and electrodes (Roeleveld et al., 1997). Consequently, local activation of the same muscle distributes within a larger area on the skin. Electrodes other than those above the active muscle portion record significant activity. Hence, watershed lines in the experimental EMG image confine large clusters of electrodes, with the inclusion of false positive pixels. The fact that local activation diffuses on the skin indicates that clusters created with the watershed algorithm does not exclude or exclude only few electrodes on the active muscle portion (false negatives). Accuracy is then balanced by the exclusion of false negatives and the inclusion of false positive pixels. The accuracy of experimental and simulated EMG segmentation is expected to vary similarly with the amplitude threshold (Fig. 4).

Results obtained for the second simulation set indicate the extent to which the segmentation accuracy is physiologically applicable. Watershed segmentation consistently identified two clusters of pixels when simulating opposite and concurrent changes in the activity level of two adjacent muscles. The estimated level greatly approached the simulated level of activation for each muscle (Fig. 5b). Conversely, unrepresentative estimates of muscles activation (Fig. 5) were obtained with the traditional technique for parameter extraction from EMG maps (Farina et al., 2008). Therefore, local variations in the level of neuromuscular activity are quantified properly with the segmentation of experimental EMG images. Actual amplitude of localized activity, however, is possibly overestimated if EMGs are recorded with considerable noise (0 dB SNR; Fig. 5a), which is often not the case (Merletti and Hermens, 2004).

4.3. Identifying localized neuromuscular activity

Multi-channel EMG recordings allow for the estimation of muscle fibers direction (Grönlund et al., 2005) and the centroid of EMG amplitude (Farina et al., 2008), for the identification of motor unit action potentials (Holobar et al., 2009), and for the robust estimation of EMG descriptors (Farina and Falla, 2008). Insights into the localized activity within and between muscles is often obtained by visual inspection of multi-channel EMGs (Troiano et al., 2008), which is time consuming and subjective. Conversely, the watershed technique holds remarkable potential for the automatic identification of active muscle portions.

Recently, Staudenmann et al. (2009) applied *K*-means clustering to identify localized activity in the calf muscles. The number of clusters was fixed to six, beforehand, to avoid the equivocal discarding of information and the identification of local minimum of distance. Some properties render the watershed algorithm more attractive than conventional clustering techniques for the automatic segmentation of EMG images: (1) the identification of clusters does not rely on distances minimization and is not supervised; (2) initial guess about the number of clusters is not required; (3) the accuracy is marginally sensitive to noise, fat thickness and electrode montage; (4) isolated pixels with high intensity, likely resulting from contact problems in the electrode–skin interface (Clancy et al., 2002), would be discarded with the gradient flattening.

The results obtained for the experimental signals recorded from MG and LG are striking. Small portions of these muscles, activated during brief plantar flexion, were tracked remarkably well with the segmentation algorithm (Fig. 7). Conventionally, the activity of gastrocnemius muscles is expected to decrease when one exerts plantar flexion with knee flexed (Arampatzis et al., 2006). EMG maps indicate that this might not be the case. The result in Fig. 7 does not allow for conclusive ascertainments concerning the load sharing between gastrocnemii. Nevertheless, it shows that both muscles are activated locally. Compelling evidences support the compartmentalization of gastrocnemius muscles and the high selectivity of surface EMGs recorded from

pinnated muscles (English et al., 1993; Wolf and Kim, 1997, Vieira et al., 2010; manuscript under preparation). Consequently, pairs of surface electrodes positioned on MG or LG unlikely provide representative recording of general muscle activity.

Watershed segmentation proved useful in distinguishing patterns of activation between proximal and distal MG regions during standing. Fluctuations in mean ARV amplitude occurred with dissimilar timing between muscle locations (compare ARV traces in Fig. 8b). Indeed, with intramuscular electrodes we observed that motor units in different portions of the MG muscle are activated with variable timing during standing (Vieira et al., 2009, 2010), suggesting a flexible and selective controller for the fine adjustments of calf muscles length with body sways (Loram et al., 2005). Although the level of gastrocnemius activation is expectedly small during standing, the equalization technique rescales EMGs amplitude to the whole spectrum of gray intensity. Slight variations in amplitude are thus emphasized. Considering that the watershed algorithm confines all regional minima in the image (Vincent and Soile, 1991; Fig. 2), clusters of activity are likely identified from equalized EMG images obtained for low-intensity contractions.

The method proposed here houses multiple noteworthy applications. For example, studies focusing on the muscle force estimation from EMGs (Lloyd and Besier, 2003), on the timing of muscle activation (Schieppati et al., 2001), on the synergic activation of muscles spanning the same joint (McLean and Goudy, 2004), or on the contribution of distinct muscles in specific motor tasks (Danion et al., 2002), would benefit from the automatic tracking of localized muscle activity.

4.4. Limitation of watershed segmentation

The watershed algorithm applies for the segmentation of images. Consequently, it requires the use of bi-dimensional grid of electrodes for the automatic identification of local EMG activity. When using a linear array or pairs of electrodes, different methods could possibly work for determining localized muscle activity (Staudenmann et al., 2009; Wolf et al., 1998).

Conflict of interest statement

None of the authors has any conflict of interest concerning the publications of this work.

Acknowledgements

T. Vieira is a recipient of a doctoral fellowship from the Brazilian National Research Council (CNPq). This study was supported by the Compagnia di San Paolo and Fondazione Cassa di Risparmio di Torino.

Appendix A. Supplementary material

Supplementary data associated with this article can be found in the online version at doi:10.1016/j.jbiomech.2010.03.049.

References

Arampatzis, A., Karamanidis, K., Stafilidis, S., Morey-Klapsing, G., DeMonte, G., Brüggemann, G., 2006. Effect of different ankle- and knee-joint positions on gastrocnemius medialis fascicle length and EMG activity during isometric plantar flexion. Journal of Biomechanics 39, 1891–1902.

Clancy, E.A., Morin, E.L., Merletti, R., 2002. Sampling, noise-reduction and amplitude estimation issues in surface electromyography. Journal of Electromyography and Kinesiology 12, 1–16.

Danion, F., Li, S., Zatsiorsky, V.M., Latash, M.L., 2002. Relations between surface EMG of extrinsic flexors and individual finger forces support the notion of muscle compartments. European Journal of Applied Physiology 88, 185–188.

Eng, J.J., Hoffer, J.A., 1997. Regional variability of stretch reflex amplitude in the cat medial gastrocnemius muscle during a postural task. Journal of Neurophysiology 78, 1150–1154.

English, A.W., Wolf, S.L., Segal, R.L., 1993. Compartmentalization of muscles and their motor nuclei: the partitioning hypothesis. Physical Therapy 73, 857–867.

Farina, D., Cescon, C., Merletti, R., 2002. Influence of anatomical, physical, and detection-system parameters on surface EMG. Biological Cybernetics 86, 445–456.

Farina, D., Falla, D., 2008. Estimation of muscle fiber conduction velocity from two-dimensional surface EMG recordings in dynamic tasks. Biomedical Signal processing and Control 3, 138–144.

Farina, D., Leclerc, F., Arendt-Nielsen, L., Buttelli, O., Madeleine, P., 2008. The change in spatial distribution of upper trapezius muscle activity is correlated to contraction duration. Journal of Electromyography and Kinesiology 18, 16–25.

Farina, D., Merletti, R., 2001. A novel approach for precise simulation of the EMG signal detected by surface electrodes. IEEE Transaction on Biomedical Engineering 48, 637–646.

Farina, D., Mesin, L., Martina, S., Merletti, R., 2004. Comparison of spatial filter selectivity in surface myoelectric signal detection—influence of the volume conductor model. Medical and Biological Engineering and Computing 42, 114–120.

Fuglevand, A.J., Winter, D.A., Patla, A.E., 1993. Models of recruitment and rate coding organization in motor-unit pools. Journal of Neurophysiology 70, 2470–2488.

Grönlund, C., Ostlund, N., Roeleveld, K., Karlsson, J.S., 2005. Simultaneous estimation of muscle fibre conduction velocity and muscle fibre orientation using 2D multichannel surface electromyogram. Medical and Biological Engineering and Computing 43, 63–70.

Heijmans, H.J.A.M., 1995. Mathematical morphology: a modern approach in image processing based on algebra and geometry. SIAM Review 37, 1–36.

Holobar, A., Farina, D., Gazzoni, M., Merletti, R., Zazula, D., 2009. Estimating motor unit discharge patterns from high-density surface electromyogram. Clinical Neurophysiology 120, 551–562.

Kim, J.Y., Kim, L.S., Hwang, S.H., 2001. An advanced contrast enhancement using partially overlapped sub-block histogram equalization. IEEE Transactions on Circuits and Systems for Video Technology 11, 475–484.

Lloyd, D.G., Besier, T.F., 2003. An EMG-driven musculoskeletal model to estimate muscle forces and knee joint moments in vivo. Journal of Biomechanics 36, 765–776.

Loram, I.D., Maganaris, C.N., Lakie, M., 2005. Human postural sway results from frequent, ballistic bias impulses by soleus and gastrocnemius. Journal of Physiology 564, 295–311.

McLean, L., Goudy, N., 2004. Neuromuscular response to sustained low-level muscle activation: within- and between-synergist substitution in the triceps surae muscles. European Journal of Applied Physiology 91, 204–216.

Merletti, R., Botter, A., Troiano, A., Merlo, E., Minetto, M.A., 2009. Technology and instrumentation for detection and conditioning of the surface electromyographic signal: state of the art. Clinical Biomechanics 24, 122–134.

Merletti, R., Farina, D., Gazzoni, M., 2003. The linear electrode array: a useful tool with many applications. Journal of Electromyography and Kinesiology 13 37–47

Merletti, R., Hermens, H.J., 2004. Detection and conditioning of the surface EMG signal. In: Merletti, R., Parker, P. (Eds.), Electromyography: Physiology, Engineering and Noninvasive Applications.. John Wiley & Sons, New Jersey, pp. 107–131.

Mesin, L., Merletti, R., Rainoldi, A., 2009. Surface EMG: the issue of electrode location. Journal of Electromyography and Kinesiology 19, 719–726.

Roeleveld, K., Stegeman, D.F., Vingerhoets, H.M., Van Oosterom, A., 1997. The motor unit potential distribution over the skin surface and its use in estimating the motor unit location. Acta Physiologica Scandinavica 161, 465–472.

Schieppati, M., Nardone, A., Corna, A., Bove, M., 2001. The complex role of spindle afferent input, as evidenced by the study of posture control in normal subjects and patients. Neurological Sciences 22, S15–S20.

Staudenmann, D., Kingma, I., Daffertshofer, A., Stegeman, D.F., Van Dieën, J.H., 2009. Heterogeneity of muscle activation in relation to force direction: a multi-channel surface electromyography study on the triceps surae muscle. Journal of Electromyography and Kinesiology 19, 882–895.

Troiano, A., Naddeo, F., Sosso, E., Camarota, G., Merletti, R., Mesin, L., 2008. Assessment of force and fatigue in isometric contractions of upper trapezius muscle by surface EMG signal and perceived exertion scale. Gait & Posture 28, 179–186.

Vieira, T.M.M., Mastrangelo, F., Merletti, R., 2008. Assessment of gastrocnemius heterogeneity using a high density SEMG system. In: Proceedings of the XVIIth Conference of the International Society of Electrophysiology and Kinesiology. Brock University, Ontario.

Vieira, T.M.M., Merletti, R., Farina, D., 2009. Intermittent recruitment of motor units in the medial gastrocnemius muscle during quiet standing. Gait & Posture 30, S17–S18.

Vieira, T.M.M., Windhorst, U., Merletti, R., 2010. Is the stabilization of quiet upright stance in humans driven by synchronized modulations of the activity of medial and lateral gastrocnemius muscles? Journal of Applied Phyisiology 108 85–97.

Vincent, L., Soile, P., 1991. Watershed in digital spaces: an efficient algorithm based on immersion simulations. IEEE Transactions on Pattern Analysis and Machine Intelligence 13, 583–598.

Wolf, S.L., Ammerman, J., Jann, B., 1998. Organization of responses in human lateral gastrocnemius muscle to specified body perturbations. Journal of Electromyography and Kinesiology 158, 11–21.

Wolf, S.L., Kim, J.H., 1997. Morphological analysis of the human tibialis anterior and medial gastrocnemius muscles. Acta Anatomica 158, 287–295.

Zajac, F.E., 1989. Muscle and tendon: properties, models, scaling, and application to biomechanics and motor control. Critical Reviews in Biomedical Engineering 17, 359–411.

Zwarts, M.J., Stegeman, D.F., 2003. Multichannel surface EMG: basic aspects and clinical utility. Muscle and Nerve 28, 1–17.